YfaE, a Ferredoxin Involved in Diferric-Tyrosyl Radical Maintenance in *Escherichia coli* Ribonucleotide Reductase†

Chia-Hung Wu,‡ Wei Jiang,§ Carsten Krebs,§,|| and JoAnne Stubbe*,‡,⊥

Departments of Chemistry and Biology, Massachusetts Institute of Technology, Cambridge, Massachusetts 02139, and Department of Biochemistry and Molecular Biology and Department of Chemistry, The Pennsylvania State University, University Park, Pennsylvania 16802

Received June 24, 2007; Revised Manuscript Received July 26, 2007

ABSTRACT: Ribonucleotide reductases (RNRs) catalyze the conversion of nucleotides to deoxynucleotides in all organisms. The class I RNRs are composed of a 1:1 complex of two homodimeric subunits: α and *β*. *β* contains the diferric-tyrosyl radical (Y•) cofactor essential for the reduction process. In vivo, the mechanism of Y• regeneration from the diferric-β_2 (met-β_2) or apo-β_2 is still unclear. Y• regenerations from met-β_2 and apo-β_2 have been designated the maintenance and biosynthetic pathways, respectively. To understand these two pathways, 181 genomes that contain *nrdAnrdB* (genes encoding α and *β*) were examined. In 29% of the cases, an open reading frame annotated 2Fe2S ferredoxin (YfaE in *Escherichia coli*) is located next to *nrdB*. Thus, YfaE has been cloned, expressed, resolubilized, reconstituted anaerobically with Fe^{2+}, Fe^{3+}, and S^{2-}, and characterized by Mössbauer, EPR, and visible spectroscopies. Titration of met-β_2 with $[2Fe2S]^{1+}$-YfaE anaerobically results in the formation of an equilibrium mixture of diferrous-β_2 and $[2Fe2S]^{2+}$-YfaE with one Fe reduced/YfaE oxidized. At the end point of the titration, O_2 is added to the mixture and the diferrous-β_2 rapidly undergoes reaction to form the diferric-Y• with a stoichiometry of 2Fe/Y• and a specific activity correlated to the amount of Y•. The reducing equivalent required for diferric-Y• cofactor biosynthesis is supplied by *β*. Under anaerobic conditions, stopped flow kinetics have been used to monitor the disappearance of the diferric cluster and the formation of $[2Fe2S]^{2+}$-YfaE. The titrations and kinetic studies provide the first evidence for a protein involved in the maintenance pathway and likely the biosynthetic pathway.

Ribonucleotide reductases (RNRs)[1] catalyze the conversion of nucleotides to deoxynucleotides in all organisms, providing the monomeric deoxynucleotides required for DNA replication and repair (*1*−*4*). The class I RNRs found in both prokaryotes and eukaryotes are composed of two subunits designated α and *β*. In prokaryotes the active form of RNR is $\alpha_2\beta_2$ (*5*), whereas in eukaryotes the active form is likely $\alpha_6\beta_6$ (*5*, *6*). α is the subunit where nucleotide reduction occurs and the site of binding of dNTP/NTP allosteric effectors that govern turnover rates and specificity of turnover. *β* is the subunit that houses a diferric-tyrosyl radical (Y•) cofactor essential for nucleotide reduction. The Y• is required to initiate the nucleotide reduction process on α, 35 Å removed (*7*, *8*). Hydroxyurea and gemcitabine are drugs presently used clinically that can reduce the Y•, inactivating *β* and consequently RNR (*5*, *9*). The importance of the diferric Y• cofactor as a therapeutic target has focused attention on the mechanism by which it is biosynthesized and maintained in an active form (*10*). We now report the discovery of a 2Fe2S ferredoxin, YfaE in *Escherichia coli* and present evidence that it plays a role in diferric-Y• cofactor maintenance and likely in diferric-Y• cofactor biosynthesis.

Seminal experiments in 1983 on crude extracts of *E. coli* suggested that enzymes (or small molecules) were present that could remove and reintroduce the Y• in *β* of RNR (*11*−*13*). The hypothesis was put forth that these molecules responsible for modulating Y• concentrations could provide an important mechanism for regulation of RNR activity (*12*, *13*). Because the relative ratios of the deoxynucleotide pools are largely governed by regulation of RNR and are largely responsible for the fidelity of DNA replication and repair, understanding the assembly and maintenance of the diferric-Y• cofactor is of great interest (*1*).

The results of the early studies, predominantly carried out by Fontecave, Reichard, and their co-workers, led to a congruent model for cluster biosynthesis and maintenance shown in Scheme 1 (*12*, *13*). The product of these pathways is the cofactor of β_2: the diferric-Y•. The early studies revealed that the Y• of the cofactor was reduced in crude cell extracts to generate met-β_2, that is, β_2 with diferric

† This work was supported by an NIH grant (GM29595 to J.S.) and the Camille and Henry Dreyfus Foundation (Teacher Scholar Award to C.K.).

* Author to whom correspondence should be addressed [telephone (617) 253-1814; fax (617) 258-7247; e-mail stubbe@mit.edu].

‡ Department of Chemistry, Massachusetts Institute of Technology.

§ Departments of Biochemistry and Molecular Biology, The Pennsylvania State University.

|| Department of Chemistry, The Pennsylvania State University.

⊥ Department of Biology, Massachusetts Institute of Technology.

[1] Abbreviations: α, ribonucleotide reductase large subunit; *β*, ribonucleotide reductase small subunit; Δ9D, delta-9 desaturase; DTT, dithiothreitol; Fd, ferredoxin; Fre, NAD(P)H:flavin oxidoreductase; apo-β_2, iron-free form of β_2; met-β_2, tyrosyl radical reduced β_2; MMO, methane monooxygenase; MMOR, methane monooxygenase reductase; RNR, ribonucleotide reductase; SF, stopped flow; $W^{+\bullet}$, tryptophan cation radical; wt, wild type; Y•, tyrosyl radical.

10.1021/bi7012454 CCC: $37.00
Published on Web 09/20/2007

Scheme 1: Proposed Pathways for Diferric-Y• Cluster Biosynthesis in β_2 and Maintenance Once the Y• Has Been Reduced in Vivo

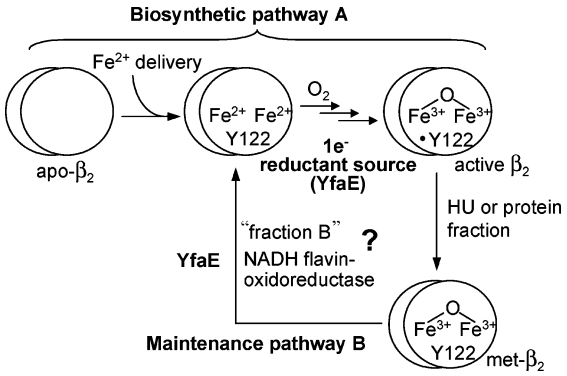

clusters and no Y• (*11*, *13*). β_2 in this state is unable to support deoxynucleotide formation. To reactivate β_2 to make deoxynucleotides, the diferric-Y• cluster would need to be assembled either de novo from apo-β_2 (biosynthetic pathway) or from met-β_2 (the maintenance pathway) (Scheme 1A,B).

The current model for the maintenance pathway is that met-β_2 is reduced to diferrous-β_2. The initial studies suggested that this reduction could be accomplished by Fre (*14*−*16*) [a ferredoxin (flavodoxin) reductase], NADPH, FAD (or FMN or riboflavin), dithiothreitol (DTT), and a "fraction B" (*12*, *13*). Despite heroic efforts, the factors in fraction B that facilitated the reduction were not successfully purified (*17*). Moreover, during the attempted purification of fraction B, Covès et al. showed that Fe^{2+} and DTT could replace the entire "fraction B" (*17*). Thus, a second model was formulated in which the Fe^{2+} in fraction B was proposed to be the likely reductant responsible for met-β_2 reduction. These studies thus called into question the role of Fre in the maintenance pathway. In contrast to the biochemical studies, the experiments in which *fre* was inactivated by transposon mutagenesis suggest an important role for this protein in maintenance of active cofactor. Hydroxyurea is known to specifically reduce the Y• of the cofactor (*9*, *18*), which inactivates RNR and results in cell death. The *fre* inactivated cells are 3 times more sensitive to hydroxyurea than the wild type (wt) cells (*19*). These growth experiments thus support a role for Fre in the maintenance pathway.

The current model for the biosynthetic pathway (Scheme 1A) is that apo-β_2 can be loaded with Fe^{2+} to form diferrous-β_2. Currently the mechanism of iron loading is not understood in vivo, whereas some information is available on Fe^{2+} loading in vitro (*20*−*22*). Once diferrous-β_2 is formed, the active diferric-Y• cofactor can be generated by the addition of O_2 and a reductant (*23*). In vitro the reducing equivalent can be supplied by Fe^{2+}, ascorbate, or mercaptoethanol, in addition to other small molecule reductants (*24*−*27*). In vivo, the factor delivering the required reducing equivalent remains to be established.

Insight into potential protein factors involved in the maintenance pathway has been provided by examination of two proteins that are structurally and functionally homologous to β_2: methane monooxygenase (MMO) and Δ^9-desaturase (Δ9D). Both enzymes use di-iron cofactors and require a similar mechanism to recycle the inactive, diferric form of the cofactor to the active, diferrous form (*28*, *29*). The MMO recycling process has been best studied and shown to use a methane monooxygenase reductase (MMOR) composed of a ferredoxin (Fd) domain and Fd reductase domain (*30*, *31*). The Fd reductase domain uses NADH to reduce its tightly bound FAD. The resulting $FADH_2$ reduces the $[2Fe2S]^{2+}$ cluster of the Fd domain, which in turn delivers the reducing equivalents required to reduce the diferric cluster of MMO to the active, diferrous form. The function of MMOR has been established as it resides within the same operon as MMO. Δ9D is also recycled from its inactive form to its active diferrous form by a plant Fd (*32*). The Fd reductase partner has not yet been identified. The diferrous forms of MMO and Δ9D react with O_2. In both cases, the cofactor acts catalytically to oxidize substrate (methane or stearoyl-ACP) to product (methanol or oleoyl-ACP). Thus, the chemistry of reduction of a diferric cluster to a diferrous cluster and reaction with O_2 parallels the maintenance pathway proposed for β_2. In the case of β_2, however, the protein itself is the substrate, generating a diferric-Y• cofactor that can then function catalytically to make deoxynucleotides.

If the catalytic cycles for MMO and Δ9D are models for cluster maintenance of β_2, a Fd might be a likely candidate to deliver the reducing equivalents required to generate diferrous-β_2 in the maintenance pathway and to supply the extra reducing equivalent in the biosynthetic pathway (Scheme 1). The analogy might further suggest that Fre could be part of a Fd reductase that acts in conjunction with a Fd. To examine these possibilities, we have searched the 181 available genomes using the database SEED for conserved genes adjacent to the *nrdAnrdB* operon coding for α_2 and β_2 for class Ia RNRs. Twenty-nine percent of the genomes have an open reading frame adjacent to the *nrdAnrdB* that is annotated as a 2Fe2S ferredoxin. In *E. coli* this gene has been designated *yfaE*. In the present studies we report cloning, expression, refolding, and purification of YfaE. The protein has been characterized by physical biochemical methods and shown to be a [2Fe2S]-Fd. The ability of the reduced form of YfaE to reduce the diferric cluster of met-β_2 has been examined by titration studies and by stopped flow spectroscopy. Reassembly of the diferrous-β_2 to the diferric-Y• β_2 has also been examined. The studies together support the importance of reduced YfaE in the maintenance pathway. The quantitative analysis demonstrates that only 2 Fe^{2+} are required per Y• generated, suggesting that β itself supplies the required reducing equivalent. A comparison of the specific activities of β_2 produced in the absence or presence of excess YfaE suggests that YfaE can also supply the extra reducing equivalent in the biosynthetic pathway.

MATERIALS AND METHODS

Genomic Analysis of Genes Contiguous to nrdAB. The genome database SEED (http://theseed.uchicago.edu) using the subsystem ribonucleotide reductase was used to analyze the genes neighboring the *nrdAB* operon. For hypothetical proteins contiguous in sequence space to *nrdAB*, the amino acid sequences were analyzed by a PHI-BLAST search to see if the open reading frames possessed interesting sequence motifs that might suggest their involvement in the biosynthesis of the diferric-Y• cofactor of β_2. For genomes that contain *nrdB* but lack contiguous *yfaE*, PHI-BLAST analysis using the conserved Cys motif ($CX_{4,5}CX_2CX_{28-35}C$) of the ferredoxin iron cluster was performed to identify other possible ferredoxins.

Cloning and Expression of YfaE. YfaE was identified in the *E. coli* K-12 genome as a putative ferredoxin and a likely candidate for involvement in diferric-Y• biosynthesis and maintenance pathways. Two primers, 5′-CCGCAAGAAT-T**CATATG**GCCCGCGTTACCCTGCG-3′ and 5′-ACTA-CAGGATCCTCACATCTCGATTTCAATATC-3′ containing *Nde*I (bold) and *Bam*HI (underlined) restriction enzyme sites were used to obtain the *yfaE* from a single colony of wt *E. coli* K-12 (Yale *E. coli* Genetic Stock Center, New Haven, CT) using Taq polymerase (Promega) and PCR (manufacturer's protocol). *yfaE* was then subcloned into pET11a (Novagen) via the *Nde*I and *Bam*HI sites using T4 DNA ligase (Promega) with a vector-to-insert ratio of 1:8. The sequence of *yfaE* was confirmed by DNA sequencing at the MIT Biopolymers Laboratory.

To express YfaE, pET11a-*yfaE* was transformed into BL21 Gold (DE3) competent cells (Stratagene) that were grown on LB plates with 100 μg/mL ampicillin. A single colony from the plate was inoculated into 5 mL of LB (100 μg/mL ampicillin in all growths), and the culture was grown at 37 °C for 6 h, transferred into 2 L of LB, and grown for an additional 16 h at 37 °C with shaking at 180 rpm. When the A_{600nm} reached ~2, the cells were harvested by centrifugation at 12000*g* for 20 min at 4 °C. The cells from 6 L of LB growth were suspended in 100 mL of 100 mM Tris-HCl/5% glycerol, pH 8.0, rapidly frozen in liquid nitrogen, and stored at −80 °C. A typical yield was ~4 g of cell paste/L of culture.

Purification of Inclusion Bodies Containing YfaE, Solubilization, Refolding, Assembly of 2Fe2S Cluster, and Purification of YfaE. To purify YfaE, the cell suspension (~20 g in 100 mL of 100 mM Tris-HCl/5% glycerol, pH 8.0**)** was thawed, and the cell walls were broken by passage twice through a French pressure cell at 16000 psi. The insoluble debris, including the inclusion bodies that were predominantly YfaE, was spun down at 17000*g* at 4 °C for 20 min. The combined pellets were suspended in 120 mL of 100 mM Tris-HCl/4% (v/v) Triton-X-100/2 M urea, pH 8.0 (*33*), by sonication at 5 W output for 1 min in an ice−water bath (VirSonic 100, SP Industries Co., Gardiner, NY). The suspension was then pelleted by centrifugation at 17000*g* and 4 °C for 20 min and the supernatant discarded. This process was repeated an additional two times. The pellet was then washed three times with 120 mL of water. The resulting inclusion bodies were stored at −20 °C. Typically ~0.1 g of inclusion bodies was obtained per gram of cell paste.

Cluster assembly of YfaE and subsequent purification of the folded, holo protein was carried out in a custom-designed glovebox (M. Braun, Newburyport, MA) in a cold room at 4 °C. All buffers and resins for chromatography were degassed on a Schlenk line (stirring and evacuation for ~1 h followed by refilling with Ar for ~15 min, three times) before being brought into the glovebox. Inclusion bodies (~0.4 g for a typical purification) were suspended in 80 mL of 100 mM Tris-HCl/8 M urea/100 mM DTT, at pH 7.8, and stirred for 1.5 h. To the solubilized protein were added 80 μL of $FeCl_3$ (100 mM stock solution in 10 mM HCl), 88 μL of $Fe(NH_4)_2(SO_4)_2$ (90 mM of stock solution in H_2O), and 160 μL of NaS (100 mM stock solution in 10 mM NaOH) over 10 min to give final concentrations of 100, 100, and 200 μM, respectively. The solution was then rapidly diluted from 80 to 320 mL with 100 mM Tris-HCl, pH 7.8, and the refolding process allowed to proceed for 18 h. The sample (320 mL) was then loaded onto a Q-Sepharose column (2.5 × 4 cm, High Performance, Pharmacia Biotech) in the glovebox at a flow rate of 3 mL/min, washed with 200 mL of 100 mM Tris-HCl, pH 7.8, and eluted with a 150 mL × 150 mL linear gradient from 0 to 1 M NaCl in 100 mM Tris-HCl, pH 7.8. Fractions of 5.5 mL were collected, and those with an $A_{340/280nm} > 0.6$ were pooled and concentrated to ~3 mL by Millipore Amicon concentrator using a 45 mm PLBC3 membrane that had previously been washed with 30 mL of 100 mM sodium dithionite, dd-H_2O, and 100 mM Tris-HCl, pH 7.8, before use. A typical elution profile is shown in the Supporting Information (Figure S1). The concentrate (3 mL) was then loaded onto a Sephadex G-75 column (2.5 × 45 cm, superfine, Sigma) at a flow rate of 25 mL/h and eluted overnight in 100 mM Tris-HCl, pH 7.8. Fractions of 6.3 mL were collected, and those with an $A_{340/280nm} > 0.7$ were pooled and concentrated as above. A typical elution profile is shown in the Supporting Information (Figure S2). The YfaE concentration was determined using $\epsilon_{420nm} = 11\ mM^{-1}\ cm^{-1}$ (*34*). The yield was typically ~60 mg of YfaE/g inclusion bodies.

Preparation of a 1:1 Mixture of $^{57}Fe^{2+}$:$^{57}Fe^{3+}$ for Mössbauer Analysis of [^{57}Fe]-YfaE. To prepare the $^{57}Fe^{3+}$ stock solution, ^{57}Fe foil (~4 mg) was added to a mixture of 375 μL of 12 N HCl and 125 μL of 13 N HNO_3 in a 10 mL pear-shaped flask for ~1 h at room temperature. The solution was then degassed in vacuo for ~1 min with stirring and brought into the glovebox. The solution was then neutralized by adding ~0.4 mL of 10 N NaOH. To prepare the $^{57}Fe^{2+}$ stock solution, ^{57}Fe foil (~8 mg) was added into 800 μL of 12 N HCl in a 10 mL pear-shaped flask fitted with a ground glass stopper. The solution was degassed immediately for ~1 min on a Schlenk line and then stirred in a 70 °C oil bath overnight with the glass stopper closed. The $^{57}Fe^{2+}$ solution was degassed again for ~1 min, brought into the glovebox, and neutralized by adding ~0.56 mL of 10 N NaOH. The concentration of each solution was determined by using the ferrozine assay (*35*) in the absence of (Fe^{2+}) or in the presence of ascorbate (Fe^{3+}), respectively. The reconstitution and purification of ^{57}Fe YfaE were then carried out as described above.

Characterization of YfaE. a. UV−Visible Spectroscopy. Purified $[2Fe2S]^{1+}$-YfaE was placed into a 0.7 mL cuvette in the glovebox and fitted with an airtight screw cap (Starna Cells, Atascadero, CA). The cuvette was removed from the glovebox, and the absorption spectrum was recorded using a Varian Cary 3 spectrophotometer (Walnut Creek, CA). The screw cap was then removed, and O_2 (Airgas, Radnor, PA) was blown over the surface of the sample for 5 s; the sample was mixed by inverting the cuvette. The spectrum was then again recorded.

b. Iron and Sulfide Quantitation. The amounts of iron (*35*) and sulfide (*36*) per YfaE were determined following the published procedures.

c. EPR Spectroscopy. The purified YfaE (1.8 mM) was placed in an EPR tube inside the glovebox and frozen in liquid nitrogen. EPR spectra were recorded using a Bruker ESP-300 X-band spectrometer at 77 K. The spin quantitation was carried out using a $CuSO_4$ standard (*37*) and Win-EPR software (Bruker).

d. Mössbauer Spectroscopy. Mössbauer spectra were recorded on spectrometers from WEB Research (Edina, MN) operating in the constant acceleration mode in transmission geometry. Spectra were recorded with the temperature of the sample at 4.2 K maintained by a liquid helium cryostat. For low-field spectra, the sample was kept inside an SVT-400 dewar (Janis, Wilmington, MA) and a magnetic field of 53 mT was applied either parallel or perpendicular to the γ-beam. For high-field spectra, the sample was kept inside a 12SVT dewar (Janis), which houses a superconducting magnet that allows for application of variable fields between 0 and 8 T parallel to the γ-beam. The isomer shifts quoted are relative to the centroid of the spectrum of a metallic foil of Fe at room temperature. Data analysis was performed using the program WMOSS from WEB Research, using the spin Hamiltonian given in eq 1, in which all symbols have their usual meaning (*38*).

$$\mathbf{H} = \beta \mathbf{S}\cdot\mathbf{g}\cdot\mathbf{B} + \sum_{i=1}^{2} \frac{eQV_{zz,i}}{4}\left[\mathbf{I}_{z,i}^{\,2} - \frac{I_i(I_i+1)}{3} + \frac{\eta}{3}(\mathbf{I}_{x,i}^{\,2} - \mathbf{I}_{y,i}^{\,2})\right] + \sum_{i=1}^{2} \mathbf{S}\cdot\mathbf{A}_i\cdot\mathbf{I}_i - \sum_{i=1}^{2} g_n\beta_n\mathbf{B}\cdot\mathbf{I}_i \quad (1)$$

Simulations of the $[2Fe2S]^{1+}$ cluster were carried out with respect to the total spin of the ground state, $S = {}^1/_2$. The **A**-tensors in eq 1 are given with respect to the total spin. They are related to the intrinsic **a**-tensors by eq 2, in which +7/3 and −4/3 are the vector coupling coefficients for the $S = {}^1/_2$ ground state (*39*, *40*).

$$\mathbf{A}_{\mathrm{Fe(III)}} = +7/3\cdot\mathbf{a}_{\mathrm{Fe(III)}} \qquad \mathbf{A}_{\mathrm{Fe(II)}} = -4/3\cdot\mathbf{a}_{\mathrm{Fe(II)}} \quad (2)$$

It was assumed that the fluctuation of the electronic states is slow compared to the ^{57}Fe Larmor frequency.

Titration of Met-β_2 with [2Fe2S]$^{1+}$-YfaE. a. Preparation of Met-β_2. Wt-β_2 [1 mL, ∼0.4 mM, specific activity of 6500 nmol/min/mg and 1.1 Y$^\bullet$ (*41*)] was incubated with 80 mM hydroxyurea (Sigma) at 30 °C for 30 min (*11*). The hydroxyurea was removed by loading ∼0.5 mL of sample onto a Sephadex G-25 column (1 × 26 cm, Sigma) in 100 mM Tris-HCl, pH 7.8. The protein-containing eluent (2 mL) was concentrated to ∼1 mL by Microcon YM30 (Millipore), degassed with stirring on a Schlenk line, and then brought into the glovebox. The concentration of the met-β_2 was determined using $\epsilon_{280\mathrm{nm}} = 131\ \mathrm{mM^{-1}\ cm^{-1}}$ (*41*). The removal of Y$^\bullet$ was confirmed by $A_{410\mathrm{nm}}$, and the iron content was determined by the ferrozine assay (*35*).

b. Reduction of Met-β_2 to Diferrous-β_2. $[2Fe2S]^{1+}$-YfaE (100 μM in 100 mM Tris-HCl, pH 7.8) was placed into a 250 μL gastight syringe fitted with a repeating dispenser (model PB600-1, Hamilton) and the needle passed through the septum (12 mm Teflon/silicon, Pierce) of the 0.7 mL cuvette. The cuvette contained 360 μL of 10 μM met-β_2 in 100 mM Tris-HCl, pH 7.8. YfaE was added in 5 μL aliquots. The spectra were recorded on a Cary 3 spectrophotometer, and a difference spectrum was recorded and examined between each titration step. The titration end point was reached when the difference spectrum indicated the presence of reduced YfaE. This experiment was repeated 10 times on two separate batches of $[2Fe2S]^{1+}$-YfaE.

c. Assembly of Diferric-Y$^\bullet$ β_2 from Diferrous-β_2. Once an end point was reached in the reduction of β_2, O_2 was blown over the solution surface for ∼5 s, and the sample was mixed by inversion of the cuvette. The spectrum was immediately recorded. The procedure was repeated, and no further change in the spectrum was observed. The amount of Y$^\bullet$ generated was determined by EPR spectroscopy, and the specific activity of the enzyme was determined by the spectrophotometric assay (*41*).

d. Calculation of Fe Reduced and YfaE Oxidized at the Titration End Point. The amount of Fe reduced during the titration is calculated by eq 3, assuming diferrous-β_2 and met-β_2 are the only forms of β_2 in the sample. There are 3.4 irons/β_2. $A_{320\mathrm{i}}$ and $A_{320\mathrm{f}}$ are the absorptions at 320 nm before and after the titration. $A_{320\mathrm{YfaE}}$ equals $[\mathrm{YfaE}]_\mathrm{f} \times \epsilon_{320\mathrm{nm}}$ [$\epsilon_{320\mathrm{nm}} = 13.3\ \mathrm{mM^{-1}\ cm^{-1}}$, based on $\epsilon_{420\mathrm{nm}} = 11\ \mathrm{mM^{-1}\ cm^{-1}}$ (*34*); $[\mathrm{YfaE}]_\mathrm{f}$ is the concentration of YfaE at the end point of the titration]. V_i and V_f are the initial and final volumes of the titration (in units of microliters). $\epsilon_{320\mathrm{diferrous}\beta2}$ and $\epsilon_{320\mathrm{met}\beta2}$ are 1.6 and 11 $\mathrm{mM^{-1}\ cm^{-1}}$, based on $\epsilon_{280\mathrm{nm}}$ of diferrous-β_2 and met-β_2 (*23*, *41*).

$$\text{nmol of Fe reduced} = 3.4V_\mathrm{f}\cdot\left[\frac{\left[A_{320\mathrm{f}} - A_{320\mathrm{YfaE}} - \left(A_{320\mathrm{i}}\cdot\frac{V_\mathrm{i}}{V_\mathrm{f}}\right)\right]}{\epsilon_{320\mathrm{diferrous}\beta2} - \epsilon_{320\mathrm{met}\beta2}}\right] \quad (3)$$

e. Reduction of Met-β_2 with YfaE and Assembly of Diferric-Y$^\bullet$ Cofactor: Analysis of Y$^\bullet$ by EPR and Activity. Met-β_2 (10 μM) was titrated with 14−200 μM YfaE in a final volume of 360 μL of 100 mM Tris-HCl, pH 7.8. The assembly of diferric-Y$^\bullet$ cofactor, EPR spectroscopic analysis, and determination of the specific activity of RNR were carried out as described above.

Quantitation of Fe^{2+} Produced by the Ferrozine Assay during Reduction of Met-β_2 with [2Fe2S]$^{1+}$-YfaE. $[2Fe2S]^{1+}$-YfaE (100 μM in 100 mM Tris-HCl, pH 7.8) was titrated anaerobically into 360 μL containing 10 μM met-β_2 and 100 μM ferrozine (100 mM Tris-HCl, pH 7.8). The amount of Fe^{2+}-ferrozine complex formed was determined using $\epsilon_{562\mathrm{nm}} = 27.9\ \mathrm{mM^{-1}\ cm^{-1}}$ (*35*). The $A_{562\mathrm{nm}}$ of Fe^{2+}-ferrozine generated concomitantly with $[2Fe2S]^{1+}$-YfaE oxidation was obtained by subtracting the $A_{562\mathrm{nm}}$ of a titration in the absence of ferrozine and thus allowed removal of the absorption features associated with YfaE and β_2.

Stopped Flow (SF) UV−Vis Spectroscopic Characterization of Met-β_2 Reduction by [2Fe2S]$^{1+}$-YfaE. The analyses of the kinetics of met-β_2 reduction were carried out using an Applied Photophysics SX20 SF spectrometer with the cell thermostated at 37 °C. The stopped flow lines were washed with 20 mL of a 100 mM dithionite solution, 20 mL of anaerobic water, and 20 mL of anaerobic 100 mM Tris-HCl, pH 7.8. Degassed met-β_2 (10 μM in 100 mM Tris-HCl, pH 7.8) was loaded into one syringe, and reduced YfaE (30−90 μM in 100 mM Tris-HCl, pH 7.8) was loaded into the second syringe in the glovebox. The connections of the syringes to the instrument were purged with nitrogen gas during the experiments. The reaction was carried out by mixing equal volumes from each syringe. The reactions were monitored at 320 and 465 nm, the reduction of the diferric cluster of met-β_2 and the oxidation of YfaE, respectively, in

the single-wavelength photomultiplier mode. Data (2000 points) were collected in a logarithmic time scale (20 s) and analyzed in KaleidaGraph (v. 3.6, Synergy Software). Typically six shots were averaged in each set of experiments.

The amplitudes of the kinetic traces at 320 and 465 nm were used to calculate the stoichiometry between the amount of YfaE oxidized and Fe reduced in met-β_2. The amount of YfaE oxidized was calculated from $\Delta A_{465nm}/(\epsilon_{465oxidizedYfaE} - \epsilon_{465reducedYfaE})$. The A_{465nm} associated with met-β_2 and diferrous-β_2 is ~2% of the total change at 465 nm and was excluded from the calculation. The amount of met-β_2 reduced was calculated from $\Delta A_{320nm}/(\epsilon_{320diferrous\beta 2} - \epsilon_{320met\beta 2})$, assuming at the end of the reaction that β_2 is in the form of either met-β_2 or diferrous-β_2. The amount of iron reduced was calculated from the amount of met-β_2 reduced times 3.4, the iron content of met-β_2 (3.4 Fe/β_2).

RESULTS

Genomic Analysis of Genes Contiguous to nrdAB. Our current model for assembly and maintenance of the diferric-Y• is shown in Scheme 1. We propose that the pathways are likely to involve a Fd, a Fd reductase, and an iron delivery system(s). In bacteria, proteins involved in metallocluster biosynthesis and repair are often organized in operons (*42*, *43*). Thus, with a bias for proteins, we decided to investigate genes located near the *nrdAB* cluster in all bacterial genomes. For this purpose we used the genomic database, SEED. Comparison of 181 bacterial genomes that have a *nrdAB* operon revealed that in 29% a gene encoding a hypothetical 2Fe2S ferredoxin was found 3′ to *nrdAB*. This gene in *E. coli* has been designated *yfaE*. For the genomes that do not have a ferredoxin adjacent to *nrdB*, a PHI-BLAST search using the YfaE sequence and the conserved ferredoxin iron binding motif ($CX_{4,5}CX_2CX_{28,35}C$) revealed that 38% contain ferredoxin-like proteins, which could function in a capacity similar to YfaE. For the remaining 33% of the genomes, alternative reductants must be available, or the maintenance pathway may not play an important physiological role.

Because of our interest in *E. coli* RNR, YfaE thus became the focus of our attention not only because of its location in the genome relative to *nrdB*, but because a BLAST search of the databases revealed that this protein has 29% sequence identity with the Fd domain of MMOR and a 29% identity with a plant Fd that reduces Δ9D. We have postulated that the reduction steps for these enzymes, mediated by a $[2Fe2S]^{1+}$-Fd, may be very similar to the maintenance pathway to regenerate active β_2 from met-β_2.

YfaE (84 amino acids) has a molecular mass of 9.3 kDa and is smaller than the Fd domain of MMOR (98 amino acids) and the plant Fd (99 amino acids). Structural and biochemical information on the Fd of MMOR or Δ9D suggests that the four cysteines of the 2Fe2S cluster are described by a $CX_4CX_2CX_{28-31}C$ fingerprint, which is also found in YfaE (*44*, *45*). After examination of additional annotated Fds in the *E. coli* genome, only the Fd in the *isc* operon, Fdx (111 amino acids), possesses a similar motif ($CX_5CX_2CX_{35}C$) (*46*).

Expression and Purification of YfaE. As a first step in studying the pathways of cluster maintenance and assembly, our efforts were focused on the expression and purification of YfaE. Whereas overexpression of YfaE was successful, in all cases the protein was found in inclusion bodies. Efforts to obtain soluble YfaE by changing the growth temperature, adding iron to the growth media, appending different affinity tags at the C or N terminus (His_6, GST, NusA) of the protein, and coexpression with *isc* operon proteins (*47*) were all unsuccessful. We thus decided to purify YfaE from inclusion bodies and refold and reassemble its 2Fe2S cluster in vitro using protocols that have been successful with other iron−sulfur-containing proteins (*48*). The inclusion bodies were purified by repeated washing and centrifugation steps and then brought into an anaerobic box and solubilized with 8 M urea. All of the steps were then carried out anaerobically, as the oxidized YfaE has a propensity to aggregate. A 1:1:2 mixture of Fe^{2+} and Fe^{3+} and sulfide was added to the denatured YfaE under anaerobic conditions, rapidly diluted, and refolded for ~18 h. The solution was then applied to a Q-Sepharose column using a salt gradient for elution (SI Figure S1). The fractions containing $[2Fe2S]^{1+}$-YfaE were pooled, concentrated, and loaded onto a Sephadex G-75 column. The desired protein eluted as a single sharp peak (SI Figure S2). The success of the purification protocol was judged by SDS-PAGE and is shown in Figure 1. ESI mass spectrometry of YfaE gave a molecular mass of 9336 Da, consistent with the presence of the 2Fe2S cluster and loss of the N-terminal methionine. Typically, 60 mg of protein, in the reduced state, can be isolated from 1 g of inclusion bodies. The protein is stable for 1 month at 4 °C in an anaerobic box.

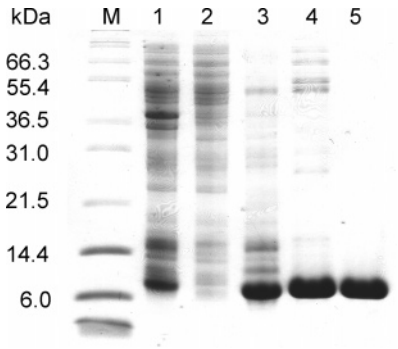

FIGURE 1: Purification of YfaE monitored by 15% SDS-PAGE. Lanes: M, molecular mass markers; 1, whole cells; 2, cell lysate; 3, purified inclusion bodies; 4, pooled protein from Q-Sepharose chromatography; 5, pooled protein from Sephadex G-75 chromatography.

$[2Fe2S]^{1+/2+}$-YfaE UV−Vis Spectrum and Sensitivity to O_2. YfaE as isolated has the absorption spectrum shown in Figure 2 (dashed line), which reveals shoulders at 350, 390, 470, and 550 nm, typical of reduced $[2Fe2S]^{1+}$ clusters (*30*). It should be noted that YfaE contains only one Trp, and thus the absorption at 280 nm is predominantly associated with the iron cluster. To characterize the oxidized state of YfaE, the protein was exposed to O_2 with stirring. The resulting spectrum is shown in Figure 2 (solid line). The oxidized form has absorption features at 340, 420, and 460 nm with a broad shoulder at 550 nm and ratios relative to A_{280nm} of 0.83, 0.60, and 0.60, respectively (*30*, *48*). This spectrum and its isosbestic point (320 nm) are typical of previously reported 2Fe2S Fds (*30*).

In contrast with many oxidized Fds, however, $[2Fe2S]^{2+}$-YfaE is not stable under aerobic or anaerobic conditions. This instability may be the result of the absence of the Fd

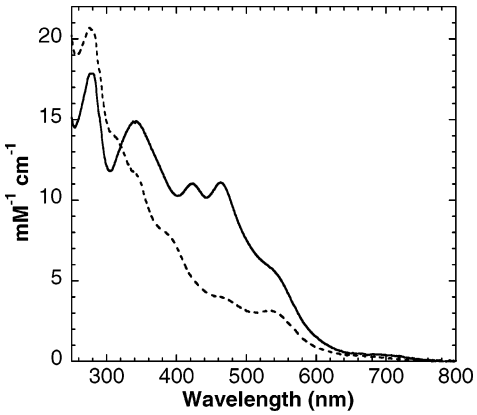

FIGURE 2: UV−visible spectra of oxidized (solid line) and reduced (dashed line) YfaE in units of mM^{-1} cm^{-1}.

reductase. At room temperature under aerobic condition, oxidized features associated with YfaE start to decrease after 1 h and disappear over a 6 h period. During the oxidation, the oxidized YfaE aggregates. The aggregate can be separated from reduced YfaE by Sephadex G-75 chromatography. Whereas sodium dithionite can reduce oxidized YfaE to its reduced state after initial exposure to O_2, it fails to regenerate reduced YfaE from the aggregates. These results were the basis for our purification and storage of YfaE in an anaerobic chamber.

Quantitation of the amount of Fe and S in the reduced YfaE requires a knowledge of the extinction coefficient for the protein. As noted above, the protein has limited 280 nm features, and thus our quantitation is based on the reported extinction coefficients for $[2Fe2S]^{2+}$ clusters at 420 nm. The numbers range from 9500 to 11000 M^{-1} cm^{-1} (*30*, *34*). All subsequent quantitation is based on the latter, with numbers based on 9500 M^{-1} cm^{-1} given in parentheses. Iron quantitation gave 2.2 ± 0.2 (1.9 ± 0.2) Fe/YfaE on the basis of seven determinations from three different batches. Sulfide quantitation gave 3.7 ± 0.2 (3.2 ± 0.2) S/YfaE on the basis of eight determinations from three different batches. The iron assay suggests the success of the reconstitution of one 2Fe2S cluster per YfaE. The iron content is also consistent with the Mössbauer analysis described subsequently. The cause of the greater than stoichiometric amount of sulfide observed is not understood, but could be associated with persulfide formation with cysteines at the C terminus of the Fd.

EPR Spectrum of $[2Fe2S]^{1+}$-YfaE. A further quantitation of the iron cluster has been made by analyzing the EPR spectrum of its reduced state. The result is shown in Figure 3. The spin quantitation using a $CuSO_4$ standard indicates 0.96 ± 0.03 (0.83 ± 0.03) spin per $[2Fe2S]^{1+}$-YfaE [*g* values of 2.036, 1.944, and 1.884, which are very similar to previously reported quantitation for the plant 2Fe2S Fd (*48*) and the Fd domain of MMOR (*30*)].

Mössbauer Spectroscopic Characterization of $[2Fe2S]^{1+}$-YfaE. The necessity of protein refolding to produce "active" YfaE required that further analysis of the cluster be obtained by Mössbauer spectroscopy. This information is also essential in eventually monitoring the kinetics of biosynthesis of the di-iron cluster of β and its maintenance. The Mössbauer spectra reveal that ~80% of total Fe is in form of a $[2Fe2S]^{1+}$ cluster and ~20% of total Fe is in the form of a $[4Fe4S]^{2+}$ cluster. From these numbers we conclude

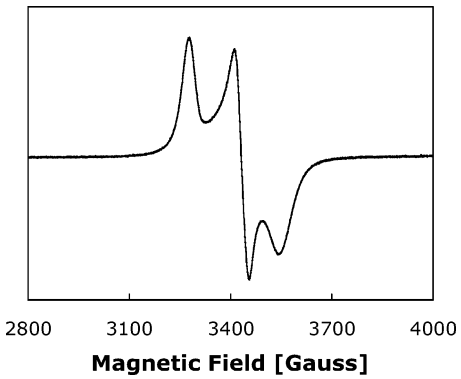

FIGURE 3: EPR spectrum at 9 GHz of $[2Fe2S]^{1+}$-YfaE (1.8 mM). Recorded at 77 K, microwave power = 1.0 mW, receiver gain = 3.17×10^4, modulation amplitude = 10 G.

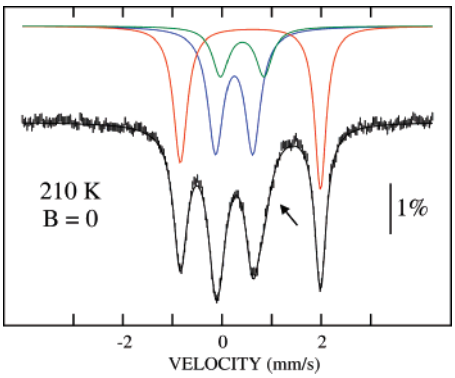

FIGURE 4: 210-K/zero-field Mössbauer spectrum of reconstituted YfaE. The solid, black line overlaid with the data is a simulation assuming three quadrupole doublets (see Table 1 for parameters). The individual contributions of the Fe^{2+} and Fe^{3+} sites of the $[2Fe2S]^{1+}$ cluster (40% each) are shown in red and blue, respectively. The contribution of the $[4Fe4S]^{2+}$ cluster (20%) is shown in green.

that 89% of YfaE harbors a $[2Fe2S]^{1+}$ cluster and 11% a $[4Fe4S]^{2+}$ cluster.[2]

The 210-K/zero-field spectrum (Figure 4) displays four lines corresponding to overlapping quadrupole doublets. The outer and inner lines have parameters reminiscent of tetrahedrally Cys_4-coordinated Fe^{2+} and Fe^{3+} sites, consistent with a $[2Fe2S]^{1+}$ cluster. The inner lines are broader and more intense, suggesting the presence of a third quadrupole doublet overlapping with the quadrupole doublet of the Fe^{3+} site. The high-energy line of the additional component can be seen as a distinct shoulder at ~1 mm/s (arrow in Figure 4). The low-energy lines of the Fe^{3+} site and the third quadrupole doublet overlap, resulting in the more intense second line. The spectrum can be analyzed as a superposition of three quadrupole doublets with parameters given in Table 1. The red and blue spectra in Figure 4 have parameters expected for the Fe^{2+} and Fe^{3+} sites of a $[2Fe2S]^{1+}$ cluster, respectively, and their relative intensity was constrained to be the same during the fit. The quadrupole doublet shown in green has parameters reminiscent of $[4Fe4S]^{2+}$ clusters.

Spectra recorded at 4.2 K in various externally applied fields corroborate this assignment. They can be analyzed as a superposition of 78% $[2Fe2S]^{1+}$ and 21% $[4Fe4S]^{2+}$

[2] To calculate the fraction of YfaE harboring a given Fe/S cluster type, the relative amount of Fe needs to be divided by the number of Fe ions found in that cluster. For example, the fraction of YfaE containing a $[2Fe2S]^{1+}$ cluster equals (80/2)/[(80/2) + (20/4)] = 8/9 ≈ 89%.

Table 1: Mössbauer Simulation Parameters of the $[4Fe4S]^{2+}$, $[2Fe2S]^{1+}$, and $[2Fe2S]^{2+}$ Clusters of YfaE[a]

sample	cluster	ground state	relative amount (%)	site	T (K)	δ (mm/s)	ΔE_Q (mm/s)	η	$\mathbf{A}/g_N\beta_N$ (T)
reconstituted YfaE	$[2Fe2S]^{1+}$	$S = 1/2$	80	Fe^{3+}	4.2	0.33	0.78	−0.6	−38.5, −37.7, −30.9
					210	0.25	0.75		
				Fe^{2+}	4.2	0.60	−3.13	−1	10.7, 10.1, 25.0
					210	0.57	2.82		
	$[4Fe4S]^{2+}$	$S = 0$	20	$Fe^{2.5}$	4.2	0.44	1.07	0	
					210	0.41	0.87		
air-oxidized YfaE	$[2Fe2S]^{2+}$	$S = 0$	>90	Fe^{3+}	4.2	0.28	0.58	nd	

[a] The g values of the $S = 1/2$ ground state of the $[2Fe2S]^{1+}$ cluster were taken from the EPR spectrum. The electric field gradient and hyperfine tensors were assumed to be collinear.

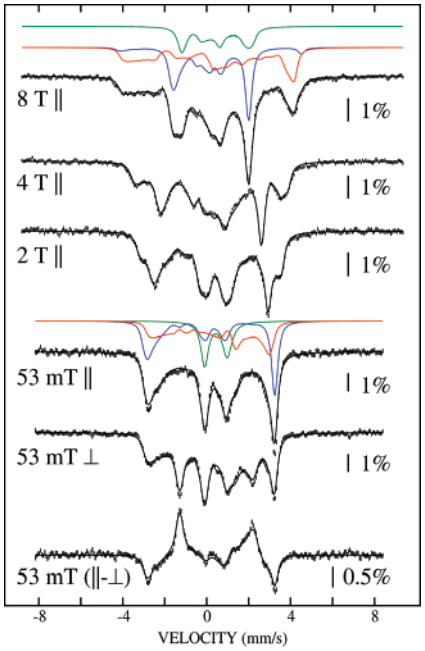

FIGURE 5: 4.2-K Mössbauer spectra of reconstituted YfaE acquired in various external magnetic fields (strength and orientation relative to the propagation direction of the γ-photons is indicated adjacent to each spectrum). The solid lines overlaid with the data are spin Hamiltonian simulations (see Table 1 for parameters). The individual contributions of the Fe^{2+} and Fe^{3+} sites of the $[2Fe2S]^{1+}$ cluster (39% each) are shown in red and blue, respectively. The contribution of the $[4Fe4S]^{2+}$ cluster (21%) is shown in green.

subspectra (Figure 5, black lines). The individual contributions of the $[4Fe4S]^{2+}$ and of the Fe^{2+} and Fe^{3+} sites of the $[2Fe2S]^{+}$ cluster are shown for the 8-T and 53-mT spectra. The simulation parameters (Table 1) are similar to those observed for other $[4Fe4S]^{2+}$ and $[2Fe2S]^{1+}$ clusters (*49*−*51*). The isomer shift values decrease with increasing temperature, due to the second-order Doppler effect (*38*), and the quadrupole splitting of the Fe^{2+} site of the $[2Fe2S]^{1+}$ cluster is slightly temperature-dependent, as was observed for the $[2Fe2S]^{1+}$ cluster from MMOR (*50*). We note that the large number of variables does not allow all parameters to be determined unambiguously.

We also considered the possibility that the YfaE sample contained oxidized $[2Fe2S]^{2+}$ cluster. This cluster form exhibits a diamagnetic ground state and thus gives rise to quadrupole doublet spectra in zero or low applied fields. High-field spectra of $[2Fe2S]^{2+}$ clusters can be predicted with good accuracy. From analysis of the spectra, we can set an upper limit of ∼7% for the fraction of $[2Fe2S]^{2+}$ in the sample. Including a small amount of this cluster type does not result in parameters significantly different from those in Table 1 and does not improve the quality of the spectral simulations. The spectrum of reconstituted YfaE that was exposed to oxygen (SI Figure S3) exhibits a quadrupole doublet with parameters typical of a $[2Fe2S]^{2+}$ cluster (Table 1). The upper limit of the fraction of Fe in the form of $[4Fe4S]^{2+}$ cluster in this sample is ∼10%, suggesting that the amount of this cluster type is variable, but small. Thus, the visible spectrum, EPR spectrum, and Mössbauer analysis suggest that the reconstitution of a folded active YfaE has been successful.

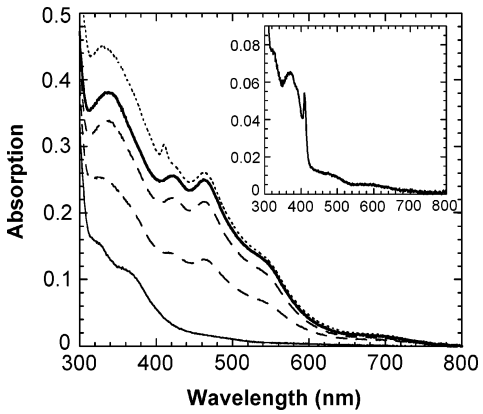

FIGURE 6: Titration of met-β_2 with $[2Fe2S]^{1+}$-YfaE under anaerobic conditions. Met-β_2 (10 μM, solid line) was titrated with 10 or 18 μM $[2Fe2S]^{1+}$-YfaE (dashed lines) to an end point with 22 μM $[2Fe2S]^{1+}$-YfaE (thick line). Upon completion of the reduction, O_2 was added to monitor cluster assembly (dotted line). (Inset) Difference spectrum between the end point of the YfaE titration and the O_2 addition.

Titration Experiments. To determine if YfaE plays a role in the maintenance pathway of the diferric-Y• cofactor of β_2 (Scheme 1), we examined the ability of $[2Fe2S]^{1+}$ to reduce met-β_2. Wt-β_2 (1.1 Y•, 3.4 Fe/β_2 and specific activity of 6500 nmol/min/mg) was reduced with hydroxyurea to produce met-β_2 (3.4 Fe/β_2). Met-β_2 in deoxygenated Tris buffer at pH 7.8 was then titrated under anaerobic conditions with $[2Fe2S]^{1+}$-YfaE. The titrations were repeated 17 times with a representative titration shown in Figure 6. The end point of the titration was assessed by monitoring the difference spectrum recorded subsequent to each addition of $[2Fe2S]^{1+}$-YfaE. When additional YfaE added remained in the reduced state, the titration was assumed to be complete. At this end point, YfaE reduced ∼2.5 Fe^{2+} of the 3.4 Fe^{3+} per met-β_2, that is, ∼75% of the total iron. Assuming that YfaE is 90−95% homogeneous on the basis of the Mössbauer, 1 YfaE

Table 2: Stoichiometry between Fe Reduced in Met-β_2 and the Amount of YfaE Oxidized

experiment	YfaE oxidized (nmol)	Fe reduced (nmol)	Fe reduced/ YfaE oxidized	activity (nmol/min/mg)	$Y^{\bullet}/\beta_2$	$Fe/Y^{\bullet}$
titration A[a]	10.3 ± 0.3	8.9 ± 1.5	0.9 ± 0.2	6200 ± 500	1.24 ± 0.04	2.0 ± 0.3
titration B[a]	9.3 ± 0.3	9.3 ± 0.7[b]	1.0 ± 0.1			
stopped flow	2.4 ± 0.6	2.4 ± 0.3	1.0 ± 0.2			

[a] Average of three titrations of met-β_2 (3.6 nmol) with $[2Fe2S]^{1+}$-YfaE in the absence (A) or in the presence (B) of ferrozine. O_2 was added at the end point of titration (A). Different batches of met-β_2 or YfaE were used in titrations A and B. [b] The amount of Fe reduced was calculated from ferrozine$-Fe^{2+}$ complex formed in the titration, assuming 1 Fe reduced per ferrozine$-Fe^{2+}$ complex formed.

Table 3: Reduction of Met-β_2 with Increasing Amounts of YfaE

met-β_2 (nmol)	YfaE (nmol)	activity (nmol/min/mg)	$Y^{\bullet}/\beta_2$	activity/($Y^{\bullet}/\beta_2$)
3.6	5	2700 ± 400	0.61 ± 0.16	4600 ± 800
3.6	10	5100 ± 200	1.16 ± 0.06	4400 ± 400
3.6	20	8200 ± 400	1.33 ± 0.05	6100 ± 400
3.6	50	9300 ± 600	1.40 ± 0.06	6800 ± 600
3.6	72	10300 ± 400	1.5 ± 0.1	6900 ± 700

reduces 1 Fe (Table 2, titration A, average of three representative titrations).

To further examine the stoichiometry of YfaE oxidation and iron reduction in met-β_2, a similar anaerobic titration in the presence of ferrozine was carried out (repeated three times) (Table 2, titration B; SI Figure S4). After subtraction of the absorption features associated with oxidized YfaE and β_2 at 562 nm, the analysis of the stoichiometry revealed that every YfaE oxidized resulted in one iron reduced. A control experiment in which YfaE was titrated into a solution with ferrozine demonstrated that the ferrous ion in $[2Fe2S]^{1+}$-YfaE is not chelated (data not shown). Results from titrations A and B (Table 2) indicate that YfaE is a chemically competent reductant of met-β_2.

Reassembly of Diferric-$Y^{\bullet}$ Cluster from Reduced Met-β_2. Once the end point for reduction of met-β_2 to the reduced state was identified under the titration conditions, O_2 was added to the cuvette and the visible spectrum recorded (Figure 6, dotted line). A difference spectrum was obtained by subtracting oxidized YfaE (amount added at the end point of the titration) from the spectrum generated in the presence of O_2. Diferric cluster absorption features at 325 and 365 nm and the $Y^{\bullet}$ features at 390 and 410 nm are readily apparent (Figure 6, inset). The amount of $Y^{\bullet}$ generated was determined by EPR spin quantitation. From titration A in which 2.5 Fe^{2+}s were generated, 1.2 $Y^{\bullet}$ were produced (Table 2). Thus, 2 Fe^{2+}s are sufficient to generate 1 $Y^{\bullet}$. Ten similar experiments were carried out, giving 2.0 ± 0.4 $Fe^{2+}/Y^{\bullet}$. Our chosen experimental conditions and a ferrozine assay established that no excess reductant (such as Fe^{2+}) was present to deliver the reducing equivalent required for cluster assembly (Scheme 1). Thus, the reducing equivalent required for cluster assembly must be derived from β itself, with the most likely candidate being the W48 (*26*, *27*).

The observation that only ~75% of the iron of met-β_2 had been reduced under these conditions suggested an equilibrium mixture of species. One would thus expect that the addition of an increased amount of YfaE would shift the equilibrium to the right, reduce more Fe^{3+}s in met-β_2, and lead to additional formation of $Y^{\bullet}$ after the addition of O_2. To test this hypothesis, met-β_2 was titrated with increasing amounts of YfaE (Table 3). The amount of Fe^{2+} could not be quantified by the spectral subtraction method (eq 3) due to the size of the extinction coefficient of $[2Fe2S]^{1+/2+}$-YfaE relative to met- and diferrous-β_2. However, spin quantitation of $Y^{\bullet}$ generated subsequent to O_2 addition (Table 3) supports this proposal.

In this same experiment with stoichiometric and excess $[2Fe2S]^{1+}$-YfaE, one might be able to obtain further insight about the source of the reducing equivalent required for cluster assembly. When no excess $[2Fe2S]^{1+}$-YfaE or Fe^{2+} is present, the reducing equivalent must come from β. However, when excess YfaE is present, it could function in this capacity. Measurement of the activity of active β_2 produced in the presence and absence of excess $[2Fe2S]^{1+}$-YfaE could provide insight as to whether $[2Fe2S]^{1+}$-YfaE could function in this capacity. One might expect that the lack of a reducing equivalent could result in activity loss due to multiple pathways for protein radical reduction, some of which could lead to altered nucleotide reduction ability. On the other hand, if $[2Fe2S]^{1+}$-YfaE is in fact the in vivo reductant, one might expect to maximize enzymatic activity. The activity assay is in general believed to be an independent measure of the $Y^{\bullet}$ concentration as previous studies have shown that the activity is directly correlated with the amount of $Y^{\bullet}$ (*52*). The specific activity per $Y^{\bullet}$ regenerated per β_2 was around 4000 nmol/min/mg per $Y^{\bullet}/\beta_2$ with stoichiometric amounts of YfaE and around 6000 nmol/min/mg per $Y^{\bullet}/\beta_2$ in the presence of excess YfaE (Table 3). Recall that the activity of the starting β_2 was 6500 nmol/min/mg (1.1 $Y^{\bullet}$s, ~6000 nmol/min/mg per $Y^{\bullet}/\beta_2$). Control experiments showed the presence of oxidized YfaE causes no significant change in the activity of β_2 (data not shown). Thus, the observed activities are in line with YfaE being able to protect β_2 from protein radical damage.

The titration studies have a number of mechanistic implications. First, the reduction of iron in β_2 by YfaE must occur cooperatively in one β. If iron was statistically reduced, the amount of $Y^{\bullet}$ recovered, which requires a diferrous-β_2, would be lower than the 2 $Fe/Y^{\bullet}$ observed. Second, diferrous-β_2 itself, upon exposure to O_2, can rapidly deliver the reducing equivalent and convert all of the reduced Fe^{2+} into differic-$Y^{\bullet}$, despite the time taken for the titrations that would potentially allow Fe^{2+} to dissociate from β. The YfaE thus may inhibit Fe^{2+} dissociation and/or enhance β's delivery of the reducing equivalent. Thus, assembly of diferrous cluster without excess reductant can now be studied. Finally, the method of cluster assembly has resulted in high levels of $Y^{\bullet}$ as well as the highest specific activities to date and suggests that if 4 Fe^{2+}s could be loaded into β_2, 2 $Y^{\bullet}$ could be generated.

The difference spectrum (Figure 6, inset) from the assembly process requires further comment. The spectrum reveals absorption features between 400 and 600 nm in addition to the diferric $Y^{\bullet}$ cofactor. We found that these

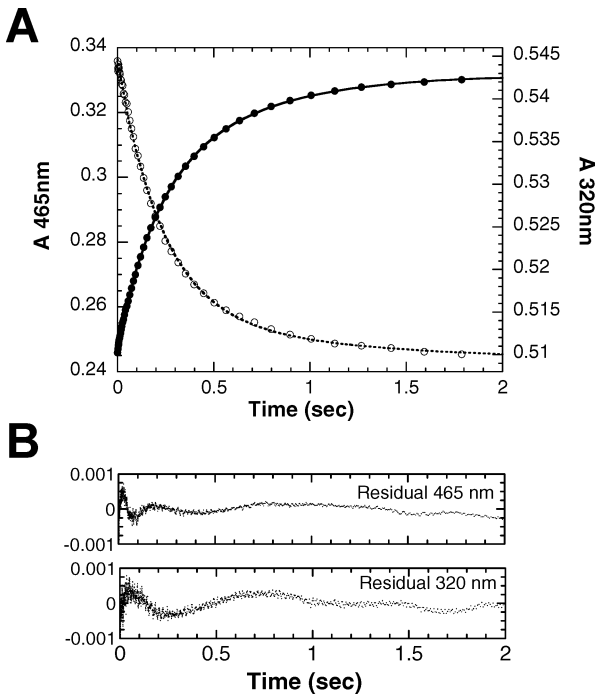

FIGURE 7: Reduction of met-β_2 (5 μM) with 37.5 μM purified $[2Fe2S]^{1+}$-YfaE monitored by stopped flow spectroscopy. (A) Oxidation of $[2Fe2S]^{1+}$-YfaE was monitored at 465 nm (solid circles); reduction of met-β_2 was monitored at 320 nm (open circles). The data were fit in both cases to biexponentials (solid line, 465 nm; dotted line, 320 nm). (B) The residuals of the fitting are shown.

features varied when different batches of YfaE were used in the titrations. Thus, these features are unlikely to be associated with an oxidized amino acid residue in β. They are most reasonably associated with the heterogeneity of the FeS clusters in YfaE from the in vitro reconstitutions and the multiple spectral subtractions required to access this spectrum.

SF Kinetics To Monitor Reduction of Met-β_2 and Oxidation of $[2Fe2S]^{1+}$-YfaE. To provide further support for the role of YfaE in vivo, the kinetics of the reduction of met-β_2 by $[2Fe2S]^{1+}$-YfaE have been examined by SF spectroscopy. The reactions were carried out under anaerobic conditions and monitored at 320 and 465 nm. Changes at 320 nm, the isosbestic point between oxidized and reduced YfaE (Figure 2), provide the best way to monitor the reduction of the diferric cluster in β_2. Oxidation of YfaE was monitored at 465 nm as this wavelength represents the biggest difference in absorption between reduced and oxidized YfaE (Figure 2).

In a typical experiment met-β_2 is mixed with variable amounts of $[2Fe2S]^{1+}$-YfaE under anaerobic conditions at 37 °C. The results of a typical experiment are shown in Figure 7. The data from analysis of the first 5 s at each wavelength were fit to two single exponentials giving rise to $k_{obs1} \sim 5\ s^{-1}$ and $k_{obs2} \sim 2\ s^{-1}$ at 465 nm and $k_{obs1} \sim 4\ s^{-1}$ and $k_{obs2} \sim 1\ s^{-1}$ at 320 nm. Under the set of conditions that we have examined, saturation of met-β_2 **(**5 μM**)** was detected at 37.5 μM YfaE (data not shown). The rate constants for reduction are considerably faster than those previously reported with Fre, fraction B, DTT, and NADPH (*13*) or with chemical reductants (*53*−*55*). These results support our proposal that YfaE can function in cluster maintenance of active β_2.

From the amplitudes of the SF data, the reaction stoichiometry between the amount of YfaE oxidized and met-β_2 reduced can also be calculated. Consistent with the titration experiments, the results suggest 1 Fe reduced per YfaE oxidized (Table 2).

DISCUSSION

The location of a putative 2Fe2S ferredoxin gene adjacent to the *nrdAnrdB* operon suggests that it might be a key player in generating and maintaining active β_2 in RNR. We have succeeded in overexpressing the *E. coli* Fd, YfaE. Purification proved to be a challenge as we were unable to obtain soluble protein under conditions we have tested. Refolding with incorporation of a homogeneous 2Fe2S cluster was also challenging, but was successful as judged by characterization of $[2Fe2S]^{1+}$-YfaE via visible, EPR, and Mössbauer spectroscopies. The extinction coefficients at 414 nm (420 nm in YfaE) for these clusters reported in the literature vary from 9500 to 11000 $M^{-1}\ cm^{-1}$ (*30*, *34*). We have used 11000 $M^{-1}\ cm^{-1}$, as it gave the best fit to all of our data: Fe stoichiometry, EPR spin quantitation, and Mössbauer quantitation. In our initial efforts to purify YfaE we took no precautions to avoid cluster oxidation. We noticed, however, that the oxidized form of YfaE aggregates irreversibly. Thus, all refolding, reconstitution, and purification steps of YfaE were carried out in a glovebox in a cold room.

Once the challenges of protein purification were overcome, we set out to address the issue of YfaE's function. Our hypothesis (Scheme 1) of YfaE's involvement in both the maintenance and biosynthetic pathways is based on the striking similarities with the structure and chemistry of Δ9D (*29*, *56*). This protein can be reduced by a plant 2Fe2S-Fd, 29% sequence identical to YfaE. Moreover, recent studies suggest that this plant Fd can reduce the diferric cluster of Δ9D through an electron-transfer pathway very similar to that proposed for β_2 in diferric-Y• assembly (*10*) [Δ9D(β_2), W62 (W48) to H146 (H118) to Fe1]. The binding site for the Fd was proposed to be adjacent to the surface exposed W62 in the vicinity of two conserved lysines (K56 and K60) in Δ9D (*32*). Interestingly, these lysines have counterparts in β_2 (K38 and K42). YfaE also shares 29% sequence identity with the Fd domain of MMOR known to reduce the inactive diferric cluster of MMO (*31*, *44*). The studies with MMOR/MMO and the Δ9D provide compelling support for our proposed function of YfaE.

To study the ability of YfaE to reduce met-β_2 to the diferrous-β_2 we carried out titrations under anaerobic conditions. These studies revealed the ability of YfaE to play this role. Quantitative analysis was also carried out using a ferrozine assay to measure the amount of Fe^{2+} generated, and the stoichiometry of the reaction confirmed that every YfaE oxidized resulted in one iron reduced (Table 2; SI Figure S4). Thus, YfaE is a chemically competent reductant of met-β_2. We also examined the ability of YfaE to reduce the diferric-Y• cofactor (data not shown). The rate of reduction is greatly reduced relative to met-β_2, and furthermore the diferric cluster is lost concomitant with Y• reduction. This behavior has been observed earlier with the chemical reductants hydrazine and phenylhydrazine (*57*) and interpreted to suggest that one Fe^{3+} is reduced to Fe^{2+} to form a transient mixed valent cluster, which is rapidly

oxidized back to the diferric cluster concomitant with $Y^{\bullet}$ reduction (*58*). The resulting met-β_2 is then rapidly reduced as described above.

After the titration end point was reached in the reduction process of met-β_2, we carried out two experiments to address the chemical competence of the resulting cluster to generate the active cofactor. In one experiment only O_2 was added, and thus the additional reducing equivalent required for cluster assembly was missing. In a second experiment we added excess $[2Fe2S]^{1+}$-YfaE followed by O_2. In both experiments, within the 2 min required to scan the spectrum, the cluster had assembled as shown by the difference spectrum (Figure 6, inset). Strikingly, this occurred in both the absence and the presence of excess reduced YfaE. These results require that the reducing equivalent is rapidly supplied by β in the former case. We generated a difference spectrum between the two experiments to look for absorption features associated with the oxidized amino acid of β providing the reducing equivalent, the putative $W48^{+\bullet}$ (*26*, *27*). These experiments resulted in variable features at $\lambda > 400$ nm due to multiple spectral subtractions and the transient nature of the protein radical.

To further characterize the resulting diferric-$Y^{\bullet}$ cofactor we have quantitated the amount of $Y^{\bullet}$ generated by EPR spectroscopy and measured the catalytic activity of the intact RNR. Interestingly, the amount of radical is half of the amount of YfaE oxidized and iron reduced, that is, 1 $Y^{\bullet}$/2 Fe. This result requires the reducing equivalent is provided by β and not by Fe^{2+} that has dissociated from β_2 during the reduction process. Finally, the amount of $Y^{\bullet}$ generated is greater than the amount of $Y^{\bullet}$ observed in a standard in vitro cofactor reconstituted β_2, suggesting that YfaE reduction will allow us to generate $Y^{\bullet}$ equivalent to the amount of Fe/2. The met-β_2 used in our experiments contained 3.4 irons. If all of the iron is reduced, then 1.7 $Y^{\bullet}/\beta_2$ should be detected. Under conditions where we have reduced 88% of the iron, we have in fact observed 1.5 $Y^{\bullet}$. Thus, it is likely that in cluster assembly the protein reduces the ferric peroxide intermediate, generating X (*22*, *59*) and $W48^{+\bullet}$ (*26*, *27*). The latter would then be rapidly reduced by YfaE, which is bound in a region of β_2 adjacent to this residue, if the analogy with Δ9D holds (*32*).

Although the titration data have clearly defined the chemically competence of YfaE, it says nothing about the kinetic competence. We thus carried out some preliminary experiments to determine the rate of reduction of met-β_2. There have been many studies investigating the reduction of met-β_2 to the diferrous-β_2 using chemical reductants and "protein reductants" (*12*, *13*, *17*, *53*−*55*). Unfortunately, the actual rate constants are not readily accessible from the published information. In the case of the chemical reductants, dithionite and a dye mediator, deazaflavin and light, DTT, and Fe^{2+} etc., the rates of reduction are very slow, on the order of several minutes (*17*, *53*−*55*). In the case of a protein reductant, Fre, a NAD(P)H:flavin oxidoreductase that was initially implicated (*12*), the reported data for reduction suggested that the rate is also very slow (<0.001 s^{-1}) (*13*, *55*). More recent studies suggest that Fre is unlikely to be directly involved in met-β_2 reduction, consistent with the slow kinetics (*17*).

We have examined the rates of met-β_2 reduction by SF kinetics monitoring both the reduction of the irons in β_2 and the oxidation of YfaE under anaerobic conditions. Because there are 3.4 irons in the met-β_2 used in this experiment and $[2Fe2S]^{1+}$-YfaE can deliver only 1 electron at a time, the kinetics by necessity are complex (*31*). Our preliminary results, however, suggest the rates are rapid, relative to those of other reductants previously reported (*13*, *54*, *55*). The data in Figure 7 have been fit for the first 5 s, during which 80% of the irons are reduced. Two single exponentials give rate constants of 4−5 and 1−2 s^{-1}. These numbers compare favorably with similar experiments that have been carried out on Δ9D and MMO. In the former case when reduced Fd is incubated with oxidized Δ9D, the rate of product production (1.5 products/dimer) is 3.4 s^{-1} (*56*). The rate-limiting step is likely the reduction step, although this has not been rigorously established. In the case of MMO, studies with the Fd domain only (residues 1−98) show that it reduces oxidized MMO with rate constants of 1 and 0.2 s^{-1} (*31*). When the three electron reduced MMOR is used, the rates are greatly increased to 95 s^{-1}, although the kinetics are complex, and 10−40% of the MMO is not reduced (*31*).

Our titration and kinetics studies together suggest we have found the correct reductant and that it is both chemically and kinetically competent. When we find the Fd reductase component, the reduction rates may increase and that YfaE will likely be used catalytically in this process. At present our protein target for this reductant is Fre as it shares 25% sequence identity with the Fd reductase domain of MMOR. Our hypothesis is that Fre may form a complex with YfaE, protecting YfaE from oxidation, and that complex formation may also result in conversion of Fre to a flavoprotein. We have generated antibodies to YfaE and will determine whether it is used catalytically in vivo. Finally, experiments with transposon insertion into Fre suggest that these bacteria are more sensitive to hydroxyurea than those with an intact *fre* (*19*). One interpretation of these results is that Fre is a missing factor in the maintenance pathway. Systematic knockout studies of each gene in the whole *E. coli* genome have reported that YfaE is not essential (*60*). This is not surprising as recent studies of Fd and other flavoproteins suggest redundancies in electron-donating pathways (*61*). If our hypothesis is correct, then studies on a Δ*yfaE*, as with Fre, should be more sensitive to hydroxyurea (*19*).

Is YfaE involved in the biosynthetic pathway? We think it is likely given the arguments above. Stopped flow experiments to monitor the assembly of the active cofactor from diferrous-β_2 with O_2 in the presence/absence of reduced YfaE are in progress to address this question.

ACKNOWLEDGMENT

We thank Dr. Viviana Izzo for help with YfaE reconstitution.

SUPPORTING INFORMATION AVAILABLE

Elution profile of Q-Sepharose chromatography of YfaE (Figure S1), elution profile of Sephadex G-75 of YfaE (Figure S2), 4.2-K/53-mT Mössbauer spectrum of a sample of reconstituted YfaE that was exposed to oxygen (Figure S3), anaerobic titration of met-β_2 with $[2Fe2S]^{1+}$-YfaE in the presence of ferrozine (Figure S4). This material is available free of charge via the Internet at http://pubs.acs.org.

REFERENCES

1. Nordlund, P., and Reichard, P. (2006) Ribonucleotide reductases, *Annu. Rev. Biochem. 75*, 681−706.
2. Jordan, A., and Reichard, P. (1998) Ribonucleotide reductases, *Annu. Rev. Biochem. 67*, 71−98.
3. Licht, S., and Stubbe, J. (1999) Mechanistic investigations of ribonucleotide reductases, in *Comprehensive Natural Products Chemistry* (Poulter, C. D., Ed.) Vol. 5, pp 163−203, Elsevier Science, New York.
4. Kolberg, M., Strand, K. R., Graff, P., and Andersson, K. K. (2004) Structure, function, and mechanism of ribonucleotide reductases, *Biochim. Biophys. Acta 1699*, 1−34.
5. Wang, J., Lohman, G. J. S., and Stubbe, J. (2007) A new paradigm for inhibition of ribonucleotide reductase: enhanced subunit interactions with substoichiometric amounts of gemcitabine-5′-diphosphate, *Proc. Natl. Acad. Sci. U.S.A.* (in press).
6. Kashlan, O. B., Scott, C. P., Lear, J. D., and Cooperman, B. S. (2002) A comprehensive model for the allosteric regulation of mammalian ribonucleotide reductase. Functional consequences of ATP- and dATP-induced oligomerization of the large subunit, *Biochemistry 41*, 462−474.
7. Uhlin, U., and Eklund, H. (1994) Structure of ribonucleotide reductase protein R1, *Nature 370*, 533−539.
8. Stubbe, J., Nocera, D. G., Yee, C. S., and Chang, M. C. Y. (2003) Radical initiation in the class I ribonucleotide reductase: long-range proton-coupled electron transfer?, *Chem. Rev. 103*, 2167−2201.
9. Brown, N. C., Eliasson, R., Reichard, P., and Thelander, L. (1969) Spectrum and iron content of protein B2 from ribonucleoside diphosphate reductase, *Eur. J. Biochem. 9*, 512−518.
10. Stubbe, J., and Riggs-Gelasco, P. (1998) Harnessing free radicals: Formation and function of the tyrosyl radical in ribonucleotide reductase, *Trends Biochem. Sci. 23*, 438−443.
11. Barlow, T., Eliasson, R., Platz, A., Reichard, P., and Sjöberg, B. M. (1983) Enzymic modification of a tyrosine residue to a stable free radical in ribonucleotide reductase, *Proc. Natl. Acad. Sci. U.S.A. 80*, 1492−1495.
12. Fontecave, M., Eliasson, R., and Reichard, P. (1987) NAD(P)H: flavin oxidoreductase of *Escherichia coli*—a ferric iron reductase participating in the generation of the free-radical of ribonucleotide reductase, *J. Biol. Chem. 262*, 12325−12331.
13. Fontecave, M., Eliasson, R., and Reichard, P. (1989) Enzymatic regulation of the radical content of the small subunit of *Escherichia coli* ribonucleotide reductase involving reduction of its redox centers, *J. Biol. Chem. 264*, 9164−9170.
14. Spyrou, G., Haggard-Ljungquist, E., Krook, M., Jornvall, H., Nilsson, E., and Reichard, P. (1991) Characterization of the flavin reductase gene (*fre*) of *Escherichia coli* and construction of a plasmid for overproduction of the enzyme, *J. Bacteriol. 173*, 3673−3679.
15. Fieschi, F., Nivière, V., Frier, C., Décout, J. L., and Fontecave, M. (1995) The mechanism and substrate specificity of the NADPH:flavin oxidoreductase from *Escherichia coli*, *J. Biol. Chem. 270*, 30392−30400.
16. Nivière, V., Fieschi, F., Décout, J. L., and Fontecave, M. (1996) Is the NAD(P)H:flavin oxidoreductase from *Escherichia coli* a member of the ferredoxin-$NADP^+$ reductase family? Evidence for the catalytic role of serine 49 residue, *J. Biol. Chem. 271*, 16656−16661.
17. Covès, J., Laulhère, J. P., and Fontecave, M. (1997) The role of exogenous iron in the activation of ribonucleotide reductase from *Escherichia coli*, *J. Biol. Inorg. Chem. 2*, 418−426.
18. Ehrenberg, A., and Reichard, P. (1972) Electron spin resonance of the iron-containing protein B2 from ribonucleotide reductase, *J. Biol. Chem. 247*, 3485−3488.
19. Covès, J., Nivière, V., Eschenbrenner, M., and Fontecave, M. (1993) NADPH-sulfite reductase from *Escherichia coli*—a flavin reductase participating in the generation of the free-radical of ribonucleotide reductase, *J. Biol. Chem. 268*, 18604−18609.
20. Umback, N. J., and Norton, J. R. (2002) Indirect determination of the rate of iron uptake into the apoprotein of the ribonucleotide reductase of *E. coli*, *Biochemistry 41*, 3984−3990.
21. Pierce, B. S., and Hendrich, M. P. (2005) Local and global effects of metal binding within the small subunit of ribonucleotide reductase, *J. Am. Chem. Soc. 127*, 3613−3623.
22. Tong, W. H., Chen, S., Lloyd, S. G., Edmondson, D. E., Huynh, B. H., and Stubbe, J. (1996) Mechanism of assembly of the diferric cluster-tyrosyl radical cofactor of *Escherichia coli* ribonucleotide reductase from the diferrous form of the R2 subunit, *J. Am. Chem. Soc. 118*, 2107−2108.
23. Atkin, C. L., Thelander, L., Reichard, P., and Lang, G. (1973) Iron and free-radical in ribonucleotide reductase—exchange of iron and Mössbauer-spectroscopy of protein-B2 subunit of *Escherichia coli* enzyme, *J. Biol. Chem. 248*, 7464−7472.
24. Bollinger, J. M., Jr., Edmondson, D. E., Huynh, B. H., Filley, J., Norton, J. R., and Stubbe, J. (1991) Mechanism of assembly of the tyrosyl radical dinuclear iron cluster cofactor of ribonucleotide reductase, *Science 253*, 292−298.
25. Bollinger, J. M., Jr., Tong, W. H., Ravi, N., Huynh, B. H., Edmondson, D. E., and Stubbe, J. (1994) Mechanism of assembly of the tyrosyl radical-diiron(III) cofactor of *Escherichia coli* ribonucleotide reductase. 2. Kinetics of the excess Fe^{2+} reaction by optical, EPR, and Mössbauer spectroscopies, *J. Am. Chem. Soc. 116*, 8015−8023.
26. Bollinger, J. M., Jr., Tong, W. H., Ravi, N., Huynh, B. H., Edmondson, D. E., and Stubbe, J. (1994) Mechanism of assembly of the tyrosyl radical-diiron(III) cofactor of *Escherichia coli* ribonucleotide reductase. 3. Kinetics of the limiting Fe^{2+} reaction by optical, EPR, and Mössbauer spectroscopies, *J. Am. Chem. Soc. 116*, 8024−8032.
27. Baldwin, J., Krebs, C., Ley, B. A., Edmondson, D. E., Huynh, B. H., and Bollinger, J. M., Jr. (2000) Mechanism of rapid electron transfer during oxygen activation in the R2 subunit of *Escherichia coli* ribonucleotide reductase. 1. Evidence for a transient tryptophan radical, *J. Am. Chem. Soc. 122*, 12195−12206.
28. Baik, M. H., Newcomb, M., Friesner, R. A., and Lippard, S. J. (2003) Mechanistic studies on the hydroxylation of methane by methane monooxygenase, *Chem. Rev. 103*, 2385−2419.
29. Fox, B. G., Lyle, K. S., and Rogge, C. E. (2004) Reactions of the diiron enzyme stearoyl-acyl carrier protein desaturase, *Acc. Chem. Res. 37*, 421−429.
30. Blazyk, J. L., and Lippard, S. J. (2002) Expression and characterization of ferredoxin and flavin adenine dinucleotide binding domains of the reductase component of soluble methane monooxygenase from *Methylococcus capsulatus* (Bath), *Biochemistry 41*, 15780−15794.
31. Blazyk, J. L., Gassner, G. T., and Lippard, S. J. (2005) Intermolecular electron-transfer reactions in soluble methane monooxygenase: a role for hysteresis in protein function, *J. Am. Chem. Soc. 127*, 17364−17376.
32. Sobrado, P., Lyle, K. S., Kaul, S. P., Turco, M. M., Arabshahi, I., Marwah, A., and Fox, B. G. (2006) Identification of the binding region of the [2Fe-2S] ferredoxin in stearoyl-acyl carrier protein desaturase: Insight into the catalytic complex and mechanism of action, *Biochemistry 45*, 4848−4858.
33. Cafaro, V., Scognamiglio, R., Viggiani, A., Izzo, V., Passaro, I., Notomista, E., Piaz, F. D., Amoresano, A., Casbarra, A., Pucci, P., and Di Donato, A. (2002) Expression and purification of the recombinant subunits of toluene/*o*-xylene monooxygenase and reconstitution of the active complex, *Eur. J. Biochem. 269*, 5689−5699.
34. Gunsalus, I. C., and Wagner, G. C. (1978) Bacterial P-450cam methylene monooxygenase components: cytochrome m, putidaredoxin, and putidaredoxin reductase, *Methods Enzymol. 52*, 166−188.
35. Fish, W. W. (1988) Rapid colorimetric micromethod for the quantitation of complexed iron in biological samples, *Methods Enzymol. 158*, 357−364.
36. Beinert, H. (1983) Semi-micro methods for analysis of labile sulfide and of labile sulfide plus sulfane sulfur in unusually stable iron−sulfur proteins, *Anal. Biochem. 131*, 373−378.
37. Broman, L., Malmström, B. G., Aasa, R., and Vanngard, T. (1962) Quantitative electron spin resonance studies on native and denatured ceruloplasmin and laccase, *J. Mol. Biol. 5*, 301−310.
38. Münck, E. (2000) in *Physical Methods in Bioinorganic Chemistry* (Que, L., Jr., Ed.) pp 287−319, University Science Books, Sausalito, CA.
39. Gibson, J. F., Hall, D. O., Thornley, J. H., and Whatley, F. R. (1966) The iron complex in spinach ferredoxin, *Proc. Natl. Acad. Sci. U.S.A. 56*, 987−990.
40. Bencini, A., and Gatteschi, D. (1990) *EPR of Exchange Coupled Systems*, Springer-Verlag, Berlin, Germany.
41. Ge, J., Yu, G., Ator, M. A., and Stubbe, J. (2003) Pre-steady-state and steady-state kinetic analysis of *E. coli* class I ribonucleotide reductase, *Biochemistry 42*, 10071−10083.
42. Casalot, L., and Rousset, M. (2001) Maturation of the [NiFe] hydrogenases, *Trends Microbiol. 9*, 228−237.

43. Johnson, D. C., Dean, D. R., Smith, A. D., and Johnson, M. K. (2005) Structure, function, and formation of biological iron−sulfur clusters, *Annu. Rev. Biochem. 74*, 247−281.
44. Müller, J., Lugovskoy, A. A., Wagner, G., and Lippard, S. J. (2002) NMR structure of the [2Fe-2S] ferredoxin domain from soluble methane monooxygenase reductase and interaction with its hydroxylase, *Biochemistry 41*, 42−51.
45. Rypniewski, W. R., Breiter, D. R., Benning, M. M., Wesenberg, G., Oh, B. H., Markley, J. L., Rayment, I., and Holden, H. M. (1991) Crystallization and structure determination to 2.5-A resolution of the oxidized [2Fe-2S] ferredoxin isolated from Anabaena 7120, *Biochemistry 30*, 4126−4131.
46. Ta, D. T., and Vickery, L. E. (1992) Cloning, sequencing, and overexpression of a [2Fe-2S] ferredoxin gene from *Escherichia coli*, *J. Biol. Chem. 267*, 11120−11125.
47. Zheng, L., Cash, V. L., Flint, D. H., and Dean, D. R. (1998) Assembly of iron-sulfur clusters. Identification of an *iscSUA-hscBA-fdx* gene cluster from *Azotobacter vinelandii*, *J. Biol. Chem. 273*, 13264−13272.
48. Cheng, H., Xia, B., Reed, G. H., and Markley, J. L. (1994) Optical, EPR, and ^{1}H NMR spectroscopy of serine-ligated [2Fe-2S] ferredoxins produced by site-directed mutagenesis of cysteine residues in recombinant Anabaena 7120 vegetative ferredoxin, *Biochemistry 33*, 3155−3164.
49. Dunham, W. R., Bearden, A. J., Salmeen, I. T., Palmer, G., Sands, R. H., Orme-Johnson, W. H., and Beinert, H. (1971) The two-iron ferredoxins in spinach, parsley, pig adrenal cortex, *Azotobacter vinelandii*, and *Clostridium pasteurianum*: studies by magnetic field Mössbauer spectroscopy, *Biochim. Biophys. Acta 253*, 134−152.
50. Fox, B. G., Hendrich, M. P., Surerus, K. K., Andersson, K. K., Froland, W. A., Lipscomb, J. D., and Münck, E. (1993) Mössbauer, EPR, and ENDOR studies of the hydroxylase and reductase components of methane monooxygenase from *Methylosinus trichosporium* Ob3b, *J. Am. Chem. Soc. 115*, 3688−3701.
51. Münck, E., Debrunner, P. G., Tsibris, J. C., and Gunsalus, I. C. (1972) Mössbauer parameters of putidaredoxin and its selenium analog, *Biochemistry 11*, 855−863.
52. Bollinger, J. M., Jr. (1993) On the chemical mechanism of assembly of the tyrosyl radical-dinulcear iron cluster cofactor of *E. coli* ribonucleotide reductase, Ph.D. Thesis, Department of Chemistry, Massachusetts Institute of Technology, Cambridge, MA.
53. Sahlin, M., Gräslund, A., Petersson, L., Ehrenberg, A., and Sjöberg, B. M. (1989) Reduced forms of the iron-containing small subunit of ribonucleotide reductase from *Escherichia coli*, *Biochemistry 28*, 2618−2625.
54. Fontecave, M., Gerez, C., Mansuy, D., and Reichard, P. (1990) Reduction of the Fe(III)-tyrosyl radical center of *Escherichia coli* ribonucleotide reductase by dithiothreitol, *J. Biol. Chem. 265*, 10919−10924.
55. Covès, J., Delon, B., Climent, I., Sjöberg, B. M., and Fontecave, M. (1995) Enzymic and chemical reduction of the iron center of the *Escherichia coli* ribonucleotide reductase protein R2. The role of the C-terminus, *Eur. J. Biochem. 233*, 357−363.
56. Lyle, K. S., Haas, J. A., and Fox, B. G. (2003) Rapid-mix and chemical quench studies of ferredoxin-reduced stearoyl-acyl carrier protein desaturase, *Biochemistry 42*, 5857−5866.
57. Han, J. Y., Swarts, J. C., and Sykes, A. G. (1996) Kinetic studies on the hydrazine and phenylhydrazine reductions of the *Escherichia coli* R2 subunit of ribonucleotide reductase, *Inorg. Chem. 35*, 4629−4634.
58. Twitchett, M. B., Dobbing, A. M., and Sykes, A. G. (2000) New mechanistic insights into the reactivity of the R2 protein of *E. coli* ribonucleotide reductase (RNR), *J. Inorg. Biochem. 79*, 59−65.
59. Yun, D., Garcia-Serres, R., Chicalese, B. M., An, Y. H., Huynh, B. H., and Bollinger, J. M., Jr. (2007) (μ-1,2-peroxo)diiron(III/III) complex as a precursor to the diiron(III/IV) intermediate X in the assembly of the iron-radical cofactor of ribonucleotide reductase from mouse, *Biochemistry 46*, 1925−1932.
60. Baba, T., Ara, T., Hasegawa, M., Takai, Y., Okumura, Y., Baba, M., Datsenko, K. A., Tomita, M., Wanner, B. L., and Mori, H. (2006) Construction of *Escherichia coli* K-12 in-frame, single-gene knockout mutants: the Keio collection, *Mol. Syst. Biol. 2*, 2006 0008.
61. Wan, J. T., and Jarrett, J. T. (2002) Electron acceptor specificity of ferredoxin (flavodoxin):NADP$^+$ oxidoreductase from *Escherichia coli*, *Arch. Biochem. Biophys. 406*, 116−126.

BI7012454